universe

MDPI

Article

Phantom Scalar Field Cosmologies Constrained by Early Cosmic Measurements

José Antonio Nájera [1,*] and Celia Escamilla-Rivera [2]

[1] Dipartimento di Fisica e Astronomia "Galileo Galilei", Università degli Studi di Padova, Via Marzolo 8, I-35131 Padova, Italy
[2] Instituto de Ciencias Nucleares, Universidad Nacional Autónoma de México, Circuito Exterior C.U., A.P. 70-543, México D.F. 04510, Mexico; celia.escamilla@nucleares.unam.mx
* Correspondence: joseantoniodejesus.najeraquintana@studenti.unipd.it

Abstract: In this work, we explore new constraints on phantom scalar field cosmologies with a scalar field employing early-time catalogs related to CMB measurements, along with the local standard observables, like Supernovae Type Ia (SNIa), $H(z)$ measurements (Cosmick clocks), and Baryon Acoustic Oscillation (BAO) baselines. In particular, we studied a tracker phantom field with hyperbolic polar coordinates that have been proposed in the literature. The main goal is to obtain precise cosmological constraints for H_0 and σ_8, in comparison to other constructions that present tension in early cosmological parameters. Our results show that phantom scalar field cosmologies have a reduced statistical tension on H_0 that it is less than 3σ using model-independent CMB catalogs as SPT-3G+WMAP9 and ACTPol DR-4+WMAP9 baselines. This suggests that these models, using a different phantom potential, might address the Hubble constant problem and reduce the systematics involved.

Keywords: dark energy; precision cosmology; cosmological parameters; Hubble constant tension

Citation: Nájera, J.A.; Escamilla-Rivera, C. Phantom Scalar Field Cosmologies Constrained by Early Cosmic Measurements. *Universe* **2024**, *10*, 232. https://doi.org/10.3390/universe10060232

Academic Editor: Jean-Michel Alimi

Received: 27 March 2024
Revised: 17 May 2024
Accepted: 20 May 2024
Published: 23 May 2024

1. Introduction

One of the first observational evidence of late-time cosmic acceleration was shown through measurements of Type Ia Supernovae (SNIa) [1,2]. Subsequently, more observables confirmed these results, e.g., the Cosmic Microwave Background (CMB) [3], Baryon Acoustic Oscillations (BAOs) [4,5], and weak gravitational lensing [6]. Moreover, the capability of SNIa to prove the cosmic acceleration is based on the facts that these objects are bright enough to be seen at a large redshift and in large quantities with a precision of $\sim$0.1 mag in brightness [7]. However, these observables have been minimized considerably by their associated statistical errors and the uncertainties in estimating cosmological parameters [8,9].

Furthermore, through the CMB temperature and polarization anisotropy observations, we have been capable of setting a strong confirmation of the standard so-called Λ-Cold Dark Matter (ΛCDM) model associated with the structure formation. This model has the advantage of explaining with high precision other observations at different redshift ranges and also explaining the effects of the cosmic acceleration through the so-called dark energy(DE). However, with the increase in surveys and their experimental sensitivity, significant cosmological statistical tensions have been rising and they are related to certain discrepancies that could be due to systematic errors or modifications (or extensions) of the standard ΛCDM model per se. While the persisting tensions of the CMB bring forth issues associated with S_8 with cosmic shear data [10], Ω_k different from zero (flat cosmology) [11,12], and A_L internal anomaly [13], the Hubble constant with local measurements, H_0 [14], is the most statistically significant tension at more than $\sim 5\sigma$. In such a case, CMB cosmological constraints, specifically, Planck constraints [15], can be obtained in a model-dependent way through the assumption of the ΛCDM model, i.e., if we change

the assumption, the constraints will change. These tensions have reached such a level of statistical significance that understanding their physics is of importance for precision cosmology. However, if these issues are not related to systematics, they could represent a crisis for the ΛCDM model, and their observational confirmation could bring a change in our current conceptions of the evolution and structure of the universe. Along with these ideas, several proposals and studies from theoretical and systematic points of view have been developed in recent years [16], and references therein. However, none of them have reached a fully solved foreground yet. This guides us to explore other schemes that could shed some light on the cosmological tensions, in particular on H_0 and σ_8 tensions.

From the survey point of view, at local scales, several missions have been working to find better cosmological constraints alongside better systematics and increasing data baselines. Some of them are large-scale structure (LSS) observations with measurements from the Dark Energy Survey (DES) [17], the Dark Energy Spectroscopic Instrument (DESI) [18], the Legacy Survey of Space and Time (LSST) on the Vera Rubin Observatory [19], and Euclid [20], among others. They have extended the concordance cosmological model to include EoS parameters of dark energy with some shifts within 1σ. At early scales, missions such as Planck 2018 [15], ACTPol DR-4 [21], and SPT-3G [22], have been working with CMB polarizations regarding in the likelihood precision measurements.

In this line of thought, an interesting path to study both the nature of dark energy and relax (or even solve) cosmological tensions, has been to directly consider the following: (i) A negative equation of state (EoS) constant value [23–25]. (ii) A dynamical EoS [26–28]. (iii) A dark energy component associated with extra terms obtained from first principles in alternative theories of gravity [29–31]. (iv) A dark energy foreground in extended theories of gravity [32] and references therein, which shows a good promise to obtain a late cosmic acceleration. In the second classification, scalar fields with kinetic terms and potentials are considered as candidates to explain the dynamics of dark energy, e.g., quintessence [33,34], *K*-essence, etc. However, neither quintessence nor K-essence is expected to resolve the H_0 tension if employed as late-time dark energy. It is expected that they make the tension even worse [35,36]. Furthermore, these examples suffer from theoretical issues where values of $w_{DE} < -1$ are not allowed. This is the so-called phantom limit. To achieve a viable evolution for dark energy, we can propose phantom models [37–39], which denote the dynamics of $w_{DE} < -1$. This kind of behavior has been studied in the literature. For instance, using CMB, BAO, and SNeIa data, it was found that the EoS of dark energy shows a phantom phase at low redshift [40]. Furthermore, using Machine Learning techniques, phantom dark energy is preferred over a cosmological constant [41]. These features could be a good landscape to address the H_0 tension. Some efforts regarding this scheme have been to propose a statistical analysis of an inverse power law quintessence model constrained by a Dark Energy Task Force simulated baseline [42], cosmological constraints on quintom tracker solutions using SNIa, BAO, and the compressed Planck likelihood [43–45], which bring high correlations with the ΛCDM model due the early times' baselines calibrated with it. Some successful scenarios include a large class of quintessence models that experiment with an early dark energy phase [46], a model that has been proposed as a solution to the Hubble tension.

Since these approaches include early-time baselines that are calibrated with the standard cosmological model, ΛCDM, in this work, we incorporated three CMB baselines that are model-independent and allowed us to obtain, in phantom scalar field cosmologies, a reduced statistical tension on H_0 that is less than 3σ for the SPT3G+WMAP9 and ACTPol+WMAP9 baselines.

This work is divided as follows: In Section 2, we summarize the reconstruction of tracker quintessence cosmologies' background and the most promising scenarios available to relax the H_0 tension. All of these cases are described through their Friedmann evolution equations. Furthermore, we consider the standard ΛCDM model in addition to these reconstructions. In Section 3, we present the statistical methodology employed for the baseline datasets mentioned. We divided our analysis into baseline (low-z) local observations and

high-z observables. Our results on new constraints and cosmological tension discussions are presented in Section 4. Finally, our conclusions are given in Section 5.

2. Phantom Scalar Field Cosmology Background

Phantom scalar field dark energy models are described by an EoS that satisfies $w < -1$ [47]. Even though current observational data have shown a good agreement with the standard cosmological model plus a cosmological constant, some of these observational baselines suggest the presence of a phantom divide boundary, i.e., dynamical dark energy proposals. This aspect could be a sign that dynamical dark energy can be constrained well by observational data. However, this denotes a big challenge in precision cosmology. Furthermore, these models have introduced scalar fields to explore the dynamics of evolving dark energy through this phantom divided line, having issues like fine-tuning. Within this scheme, tracker scenarios have been considered [48,49] where the scalar field controls the energy density and reproduces attractor background solutions, which can be constrained with local observations. In this work, we will study the parametrizations proposed in [50] and, in particular, the phantom scalar field dark energy model proposed in [51]. Considering several CMB baselines, we will verify if this model can solve (or relax) the H_0 tension. We will employ model-independent CMB experiments, and, for comparison, we include Planck 2018 constraints [15] since this baseline is calibrated with the standard ΛCDM model.

To incorporate a phantom scalar field term, we start with a gravitational action given by

$$S = \int d^4x\sqrt{-g}\left(-\frac{R}{16\pi G} + \mathcal{L}_\phi(\phi, \partial_\mu\phi) + \mathcal{L}_m\right), \tag{1}$$

where R is the Ricci scalar, G is Newton's gravitational constant, $\mathcal{L}_\phi$ is the scalar field Lagrangian (for a phantom scalar field, it is given by $\mathcal{L}_\phi = -1/2\partial^\mu\phi\partial_\mu\phi - V(\phi)$ where $V(\phi)$ is the potential of the scalar field), and $\mathcal{L}_m$ is the matter Lagrangian. We will work in a flat Friedman–Lemaître–Robertson–Walker (FLRW) metric. By varying the action (1) with respect to the FLRW metric and to the scalar field ϕ and setting it to zero, we obtain the following Friedmann equations:

$$H^2 = \frac{8\pi G}{3}(\rho + \rho_\phi), \tag{2}$$

$$\dot{H} + H^2 = -\frac{4\pi G}{3}(\rho + 3p + \rho_\phi + 3p_\phi), \tag{3}$$

$$\dot{\rho} + 3H(\rho + p) = 0, \tag{4}$$

and the Klein–Gordon equation for the scalar field given by

$$\ddot{\phi} + 3H\dot{\phi} - \frac{\partial V}{\partial\phi} = 0, \tag{5}$$

where ρ and p are the density and pressure of the matter species, and ρ_ϕ and p_ϕ the density and pressure of the scalar field ϕ. The density and pressure of the phantom scalar field are given by

$$\rho_\phi = -\frac{1}{2}\dot{\phi}^2 + V(\phi), \qquad p_\phi = -\frac{1}{2}\dot{\phi}^2 - V(\phi), \tag{6}$$

and, as we can see, these fields give rise to an equation of state $w < -1$. In this framework, it is customary to consider a new set of hyperbolic polar coordinates which ease the numerical computations [51]:

$$x = \sqrt{\frac{8\pi G}{6}}\frac{\dot{\phi}}{H} = \sqrt{\Omega_\phi}\sinh(\theta_\phi/2), \qquad y = \sqrt{\frac{8\pi G V}{3}}\frac{1}{H} = \sqrt{\Omega_\phi}\cosh(\theta_\phi/2), \quad (7)$$

$$y_1 = -2\frac{\sqrt{2}}{H}\frac{\partial\sqrt{V}}{\partial\phi}, \qquad y_2 = -\frac{4}{H}\sqrt{\frac{3}{8\pi G}}\frac{\partial^2\sqrt{V}}{\partial\phi^2}, \quad (8)$$

which enable us to rewrite the Klein–Gordon Equation (5) as

$$\Omega'_\phi = 3aH\Omega_\phi[w_{\rm tot} + \cosh(\theta_\phi)], \quad (9)$$

$$\theta'_\phi = -aH\left[3\sinh(\theta_\phi) + y_1\right], \quad (10)$$

$$y'_1 = aH\left[\frac{3}{2}(1+w_{\rm tot})y_1 + y_2(\Omega_\phi, \theta_\phi, y_1)\right], \quad (11)$$

where the prime $'$ denotes the derivative with respect to conformal time. Furthermore, $w_{\rm tot} = p_{\rm tot}/\rho_{\rm tot}$ is the total EoS including the matter species and the scalar field density and pressure. It should be noted that, in this set of variables, we need to specify the function y_2, which is equivalent to specifying the potential $V(\phi)$. Moreover, by using the definitions of scalar field density and pressure (6), we obtain

$$\rho_\phi = \frac{3H^2\Omega_\phi}{8\pi G}, \qquad p_\phi = -\rho_\phi\cosh(\theta_\phi). \quad (12)$$

Then, Ω_ϕ is the density parameter for the phantom scalar field. On the other hand, the EoS of this field is given by $w_\phi = -\cosh(\theta_\phi)$. The remaining part to solve the differential equations is to determine y_2. A parametrization can be considered [43,50]:

$$y_2 = y\left(\alpha_0 + \alpha_1\frac{y_1}{y} + \alpha_2\frac{y_1^2}{y^2}\right), \quad (13)$$

where y is given by Equation (7) and α_0, α_1, and α_2 are free parameters of the phantom field. This form of y_2 allows us to consider a wide variety of potentials like thawing and freezing potentials [50] depending on the values of the free parameters $\alpha_0, \alpha_1, \alpha_2$.

However, even with this proposal, it was found that this kind of phantom model does not address the Hubble constant problem when considering a compressed Planck likelihood. This analysis gave a Hubble value of $H_0 = 69.1^{+0.5}_{-0.6}$ km/s/Mpc [51], which is in a 3σ C.L. tension with the latest result from the SH0ES collaboration [52]. This work will reconstruct the constraints using the full Planck [15] likelihood. Furthermore, we will compare this constraint with the ones using model-independent CMB baselines. Within the baselines under consideration, we have the ACTPol DR-4 [21], the SPT-3G [22], and the WMAP9 [53] datasets. This will determine whether a phantom scalar field model like this can predict a larger late-time expansion of the universe than ΛCDM.

3. Methodology

To solve the above equations, we used our modified version of the Boltzmann code `CLASS` (https://lesgourg.github.io/class_public/class.html (accessed on 5 May 2022)) [54], interfaced to the sampling code `MontePython` (https://github.com/brinckmann/montepython_public (accessed on 5 May 2022)) [55,56]. One common core of the code is the initial conditions to perform the integrals, which were suggested in [51]. Following this suggestion, we considered the following initial conditions for θ_ϕ, y_1, and Ω_ϕ:

$$\cosh(\theta_{\phi i}) = 1 + \frac{2}{3\alpha_2}, \qquad y_{1i} = -3\sinh(\theta_{\phi i}), \qquad \Omega_{\phi i} = A\Omega_{\phi 0}a_i^{4(1+1/(2\alpha_2))}\left(\frac{\Omega_{m0}}{\Omega_{r0}}\right)^{1+1/(2\alpha_2)}, \quad (14)$$

where the sub-index 0 means at the present time. Ω_{m0}, Ω_{r0}, and $\Omega_{\phi 0}$ are the matter, radiation and phantom scalar field density parameters at the current time. a_i is the scale factor at which `CLASS` starts the integration. We select $a_i = 10^{-14}$ by default. However, an important difference in our numerical code adaption is that we did not include the presence of a cosmological constant Λ. Thus, we are letting the phantom scalar field drive the cosmic late-time accelerated expansion. Furthermore, A is a tuning parameter, which varies until we satisfy the closure relation $\Omega_{r0} + \Omega_{m0} + \Omega_{\phi 0} = 1$. We consider a universe filled with matter, radiation, and a phantom scalar field.

Observational Baselines

Our study is based on constraining the full tracker phantom model using two kinds of baseline: late-time and early-time surveys. According to this division, we can consider the following:

- Late-time baselines:
  1. **Supernovae Type Ia (SNIa) Pantheon:** We used the 1048 data points provided by the *Pantheon* [57]. This baseline measures the apparent distance for several SNIa events in $0.01 < z < 2.3$. Furthermore, this catalog provides SN magnitudes corrected for stretch and color effects along with the maximum brightness, the mass of the host galaxy, and sky position bias. To compute a cosmological useful quantity, we can calculate the distance modulus $\mu = m - M$, where m is the apparent magnitude, and M is the absolute magnitude that is considered a fixed value for our analyses. Furthermore, the $\chi^2_{\rm SN}$ for the Pantheon sample is
  $$\chi^2_{\rm SN} = \Delta\mu(z_i,\Theta)^T C^{-1}_{\rm SN} \Delta\mu(z_i,\Theta) + \ln\left(\frac{S}{2\pi}\right) - \frac{k^2(\Theta)}{S}, \tag{15}$$
  where $C^{-1}_{\rm SN}$ is the total covariance matrix for the data, Θ is the model vector parameter, S is the sum of all components of the inverse of the matrix, and $k(\Theta) = \Delta\mu(z_i,\Theta)^T C^{-1}_{\rm SN}$, using $\Delta\mu(z_i,\Theta) = \mu(z_i,\Theta) - \mu_{\rm obs}(z_i)$. Furthermore, the distance modulus $\mu(z)$ can be computed using the expression
  $$\mu(z_i,\Theta) = 5\log[D_L(z_i,\Theta)] + M, \tag{16}$$
  and where $D_L(z_i,\Theta)$ is the luminosity distance given as
  $$D_L(z_i,\Theta) = c(1+z_i)\int_0^{z_i} \frac{dz'}{H(z',\Theta)}, \tag{17}$$
  where c is the speed of light and $H(z_i,\Theta)$ is the Hubble parameter.
  2. **Cosmic clocks (CCs):** This sample offers a good tool to constrain the Hubble rate $H(z)$ at different z. To this end, the final catalog considered came from the differential age method [58]. In particular, we considered the Cosmick clocks 2016 catalog [59]. The CC method consists of using spectroscopic dating techniques on passively-evolving galaxies to compute the age difference between two galaxies at different z. By measuring this age difference, $\Delta z/\Delta t$, we can compute $H(z) = -(1+z)^{-1}\Delta z/\Delta t$. For our MCMC analysis, we computed $\chi^2_{\rm CC}$ to compare the agreement between the theoretical Hubble parameter values $H(z_i,\Theta)$, with model parameters Θ, and the observational Hubble data values $H_{\rm obs}(z_i)$, with an observational error of $\sigma_H(z_i)$. Therefore, the $\chi^2_{\rm CC}$ is calculated using the following expression:
  $$\chi^2_{\rm CC} = \sum_{i=1}^{31} \frac{\left(H(z_i,\Theta) - H_{\rm obs}(z_i)\right)^2}{\sigma^2_H(z_i)}. \tag{18}$$

3. **Baryon Acoustic Oscillations (BAOs):** In this work, we included measurements of the Hubble parameter and the corresponding comoving angular diameter at $z_{\rm eff} = 0.38, 0.51$, which were obtained from the third generation of the SDSS mission (SDSS BOSS DR12) [60]. For this BAO baseline, we computed the Hubble distance $D_H(z)$ given by $D_H(z) = \frac{c}{H(z)}$. We also used the angular diameter distance $D_A(z)$ given by

$$D_A(z) = \frac{c}{1+z}\int_0^z \frac{dz'}{H(z')}, \tag{19}$$

where the first is the comoving angular diameter distance D_M given trough $D_M = (1+z)D_A(z)$, and the second one is the volume average distance given by

$$D_V(z) = (1+z)^2\left[D_A(z)^2\frac{cz}{H(z)}\right]^{\frac{1}{3}}. \tag{20}$$

Afterwards, we calculated the corresponding combination of results $G(z_i) = D_V(z_i)/r_s(z_d)$, $r_s(z_d)/D_V(z_i)$, $D_H(z_i)$, $D_M(z_i)(r_{s,\rm fid}(z_d)/r_s(z_d))$, $H(z_i)(r_s(z_d)/r_{s,\rm fid}(z_d))$, and $D_A(z_i)(r_{s,\rm fid}(z_d)/r_s(z_d))$. For this, we required the comoving sound horizon at the end of the baryon drag epoch at $z_d \sim 1059.94$ [15], which can be calculated through

$$r_s(z) = \int_z^\infty \frac{c_s(\tilde{z})}{H(\tilde{z})/H_0}\,{\rm d}\tilde{z} = \frac{1}{\sqrt{3}}\int_0^{1/(1+z)} \frac{{\rm d}a}{a^2 H(a)\sqrt{1+\left[3\Omega_{b,0}/(4\Omega_{\gamma,0})\right]a}}, \tag{21}$$

where $c_s(z)$ is the sound speed, and we have considered a fiducial value of $r_{s,\rm fid}(z_d) = 147.78, {\rm Mpc}$ [15] with an assumption of $\Omega_{b,0} = 0.02242$ [15] and $T_0 = 2.7255$. The corresponding χ^2 is given by

$$\chi^2_{\rm BAO}(\Theta) = \Delta G(z_i,\Theta)^T C^{-1}_{\rm BAO}\Delta G(z_i,\Theta) \tag{22}$$

where $\Delta G(z_i,\Theta) = G(z_i,\Theta) - G_{\rm obs}(z_i)$ and $C_{\rm BAO}$ is the corresponding covariance matrix for the BAO observations.

- Early-time baselines:
  1. **Planck 2018:** For these CMB observations, we took the high-ℓ TTTEE, low-ℓ EE, low-ℓ TT, and lensing likelihoods [15]. Furthermore, polarization and temperature TT-TE-EE baselines were used at high multipole likelihood `Plik` $30 < \ell < 2500$ and at low multipoles TT-EE for $0 < \ell < 30$.
  2. **SPT-3G:** We also used the CMB polarization observations from the SPT-3G detector [22]. To use this data, we took the `MontePython` likelihood for SPT-3G devised in [61].
  3. **ACTPol DR-4:** This is the third CMB catalog considered coming from the Data Release 4 measured by the Atacama Telescope (ACT) Collaboration [21]. To use this catalog along with `MontePython`, we utilised the `pyactlike` Python package devised by the ACT Collaboration (https://github.com/ACTCollaboration/pyactlike (accessed on 21 April 2022)). This likelihood also includes a Gaussian prior on $\tau = 0.06 \pm 0.01$.
  4. **WMAP9:** The final CMB catalog was the Wilkinson Microwave Anisotropy Probe and we took the results from the ninth year [53]. To use this catalog along with others in MontePython, we used the `clik` software 16.0 (https://github.com/benabed/clik (accessed on 12 March 2024)) that enabled us to install the WMAP9 likelihood and use it inside MontePython.

To sample the cosmological parameters of our tracker models, we considered three different baselines for the catalogs described:

1. Planck 2018+BAO+Pantheon+Cosmic clocks;
2. SPT-3G+WMAP9+BAO+Pantheon+Cosmic clocks;
3. ACTPol DR-4+WMAP9+BAO+Pantheon+Cosmic clocks.

As we can notice, we included BAO, Pantheon, and Cosmick clocks in our three combinations. In addition to this, we varied the CMB catalogs. Planck data was included in the first combination but not in the other ones to have two Planck-independent combinations to see if this improved or changed the convergence of the scalar field and cosmological free parameters with particular emphasis on the Hubble parameter at $z = 0$, H_0.

4. Cosmological Tensions Analysis

We ran Monte Carlo Markov Chain (MCMC) methods to constrain the cosmological parameters. Furthermore, we repeated this analysis for both the tracker scalar field and the ΛCDM model to compare their performances. Moreover, we checked whether the tracker models reduced the H_0 tension compared to the last result from the SH0ES collaboration [52]. For a statistical comparison between models, we computed the Hubble tension with

$$T_{H_0} = \frac{|H_{0\,\mathrm{SH0ES}} - H_{0\,\mathrm{model}}|}{\sqrt{\sigma^2_{H_0\,\mathrm{SH0ES}} + \sigma^2_{H_0\ \mathrm{model}}}}. \tag{23}$$

We sampled the cosmological parameters using the Metropolis–Hastings method and used Gelman–Rubin's convergence criterion $R - 1 < 0.03$ [62].

We sampled over the free parameters $100\omega_b, \omega_{\mathrm{cdm}}, 100\theta_s, \ln(10^{10}A_s), n_s$, and τ_{reio}, the free scalar field parameters α_0, α_1, and α_2, and the nuisance parameters of the experiments considered and the derived parameters z_{reio}, YHe, $H_0, 10^9 A_s, \sigma_8$, and Ω_m. For the scalar field parameters, we considered uniform prior probabilities $\alpha_0 = [-12, 12], \alpha_1 = [-8, 8]$, and $\alpha_2 = [1, 16]$. These ranges were also considered to study tracker scalar field models [51]. Moreover, these priors also simplified the shooting `CLASS` method to compute the value of the derived parameter Ω_ϕ [51], and they were also consistent with the expected values of the potentials reported in [50].

We present the mean values along with the 1σ C.L. uncertainties of the cosmological parameters for the phantom scalar field model and ΛCDM model in Tables 1 and 2, respectively. We report the results for the three baselines that we considered: Planck 2018+BAO+Pantheon+Cosmic clocks, STP-3G+WMAP9+BAO+Pantheon+Cosmic clocks, and ACTPol DR-4+WMAP9+BAO+Pantheon+Cosmic clocks. We also computed the tension between the Hubble constant derived from the MCMC and the latest SH0ES value of H_0 [52]. In Figures 1 and 2, we show the confidence contours at 1σ and 2σ for the cosmological parameters and the phantom scalar field and ΛCDM, respectively.

Table 1. Mean values and uncertainties at 1σ C.L. for the phantom scalar field parameters. It should be noted that we included $10^9 A_s$ as a derived parameter instead of the traditional $\ln(10^{10}A_s)$. We present the results for our three baselines for comparison between different CMB catalogs: Planck 2018+BAO+Pantheon+Cosmic clocks, SPT-3G+WMAP9+BAO+Pantheon+Cosmic clocks, and ACTPol DR-4+WMAP9+BAO+Pantheon+Cosmic clocks. We abbreviated the late-time catalogs (BAO+Pantheon+Cosmic clocks) as Late.

Parameter	Planck 2018+Late	SPT-3G+WMAP9+Late	ACTPol DR-4+WMAP9+Late
ω_{cdm}	$0.1196^{+0.00097}_{-0.00096}$	$0.1179^{+0.0015}_{-0.0016}$	0.1208 ± 0.0015
$100\omega_b$	2.241 ± 0.014	2.265 ± 0.022	2.239 ± 0.0019
$100\theta_s$	$1.042^{+0.00028}_{-0.00029}$	$1.04^{+0.00063}_{-0.00065}$	$1.043^{+0.00059}_{-0.0006}$
n_s	0.9668 ± 0.0038	$0.9741^{+0.0065}_{-0.0067}$	$0.9731^{+0.0046}_{-0.0045}$
τ_{reio}	$0.05506^{+0.007}_{-0.0075}$	$0.07805^{+0.011}_{-0.012}$	$0.06893^{+0.0072}_{-0.0075}$

Table 1. *Cont.*

Parameter	Planck 2018+Late	SPT-3G+WMAP9+Late	ACTPol DR-4+WMAP9+Late
α_0	$1.083^{+11}_{-3.9}$	$5.567^{+6.4}_{-1.6}$	$5.462^{+6.5}_{-1.6}$
α_1	$1.04^{+7}_{-2.5}$	$4.603^{+3.4}_{-0.77}$	$5.007^{+3}_{-0.71}$
α_2	$11.29^{+4.7}_{-1.5}$	$4.061^{+0.79}_{-0.85}$	$3.147^{+0.6}_{-0.53}$
z_{reio}	7.731 ± 0.73	$9.809^{+1.1}_{-1}$	$9.114^{+0.7}_{-0.68}$
YHe	$0.2479 \pm (5.9 \times 10^{-5})$	$0.248 \pm (9.3 \times 10^{-5})$	$0.2478^{+8.1 \times 10^{-5}}_{-7.9 \times 10^{-5}}$
H_0	$68.71^{+0.48}_{-0.57}$	$70.01^{+0.55}_{-0.6}$	$69.87^{+0.55}_{-0.61}$
$10^9 A_s$	$2.103^{+0.029}_{-0.031}$	$2.195^{+0.05}_{-0.055}$	$2.185^{+0.032}_{-0.033}$
σ_8	$0.815^{+0.0062}_{-0.0064}$	0.8291 ± 0.012	$0.8416^{+0.0093}_{-0.0096}$
Ω_m	0.301 ± 0.006	$0.2868^{+0.0069}_{-0.0072}$	$0.2933^{+0.007}_{-0.0071}$
T_{H_0}	4.01	2.80	2.92

Table 2. Mean values and uncertainties at 1σ C.L. for the ΛCDM cosmological parameters. It should be noted that we included $10^9 A_s$ as a derived parameter instead of the traditional $\ln(10^{10} A_s)$. We present the results for the same baselines as for the phantom scalar field for comparison.

Parameter	Planck 2018+Late	SPT-3G+WMAP9+Late	ACTPol DR-4+WMAP9+Late
ω_{cdm}	0.1191 ± 0.00094	0.1172 ± 0.001	$0.1186^{+0.0013}_{-0.0014}$
$100\omega_b$	2.246 ± 0.014	$2.261^{+0.02}_{-0.021}$	$2.243^{+0.018}_{-0.019}$
$100\theta_s$	1.042 ± 0.00029	$1.041^{+0.00064}_{-0.00063}$	$1.043^{+0.00061}_{-0.0006}$
n_s	$0.9681^{+0.0037}_{-0.0039}$	$0.976^{+0.0062}_{-0.0063}$	$0.9764^{+0.0044}_{-0.0045}$
τ_{reio}	$0.05707^{+0.0069}_{-0.008}$	0.08415 ± 0.012	$0.07108^{+0.0075}_{-0.0076}$
z_{reio}	$7.92^{+0.71}_{-0.76}$	$10.36^{+1.1}_{-1}$	$9.279^{+0.72}_{-0.69}$
YHe	$0.2479 \pm (5.9 \times 10^{-5})$	$0.2479^{+8.7 \times 10^{-5}}_{-8.9 \times 10^{-5}}$	$0.2479^{+7.8 \times 10^{-5}}_{-8 \times 10^{-5}}$
H_0	$67.85^{+0.41}_{-0.43}$	$68.17^{+0.4}_{-0.43}$	$68.26^{+0.55}_{-0.56}$
$10^9 A_s$	$2.109^{+0.029}_{-0.033}$	$2.22^{+0.05}_{-0.056}$	$2.183^{+0.033}_{-0.034}$
σ_8	$0.8102^{+0.006}_{-0.0064}$	0.8254 ± 0.011	$0.8263^{+0.0083}_{-0.0082}$
Ω_m	$0.3075^{+0.0057}_{-0.0056}$	$0.301^{+0.0054}_{-0.0053}$	$0.3028^{+0.0073}_{-0.0076}$
T_{H_0}	4.87	4.60	4.28

As we can see, the three phantom scalar field parameters do not converge well for the compressed Planck 2028 baseline. However, the confidence contours show that they tend to have high values. For the remaining baselines, the parameter α_2 is well constrained. However, the other two have high values as in the case of the Planck baseline. The rest of the cosmological parameters show good convergence. From the CMB catalogs considered in this work, Planck has the heavier baseline. Thus, we expect its confidence contours to be the smallest. We can see in Figures 1 and 2 that this is indeed the case.

When considering the phantom scalar field, the Hubble tension gets reduced for the three baselines. However, for the Planck+Late baseline, it is still higher than 4σ C.L. It should be noted that this is different from the result from [51], where they obtained $T_{H_0} = 3.63$ using a compressed Planck likelihood. However, in our results, by using the full Planck likelihood alongside late-time data, we notice that these phantom dark energy models do not address the Hubble tension. However, the tension was reduced considerably for the remaining baselines that did not include Planck. Furthermore, it is interesting that the tension got below the 3σ C.L. This shows that tracker phantom scalar field dark energy models can reduce the Hubble constant tension for CMB baselines that do not include the Planck likelihood. For these kinds of models, $w < -1$ can produce a larger late-time expansion of the universe and, thus, a higher value of H_0 [63]. However, this particular model cannot fully solve the problem since its tension is higher than 2σ C.L.

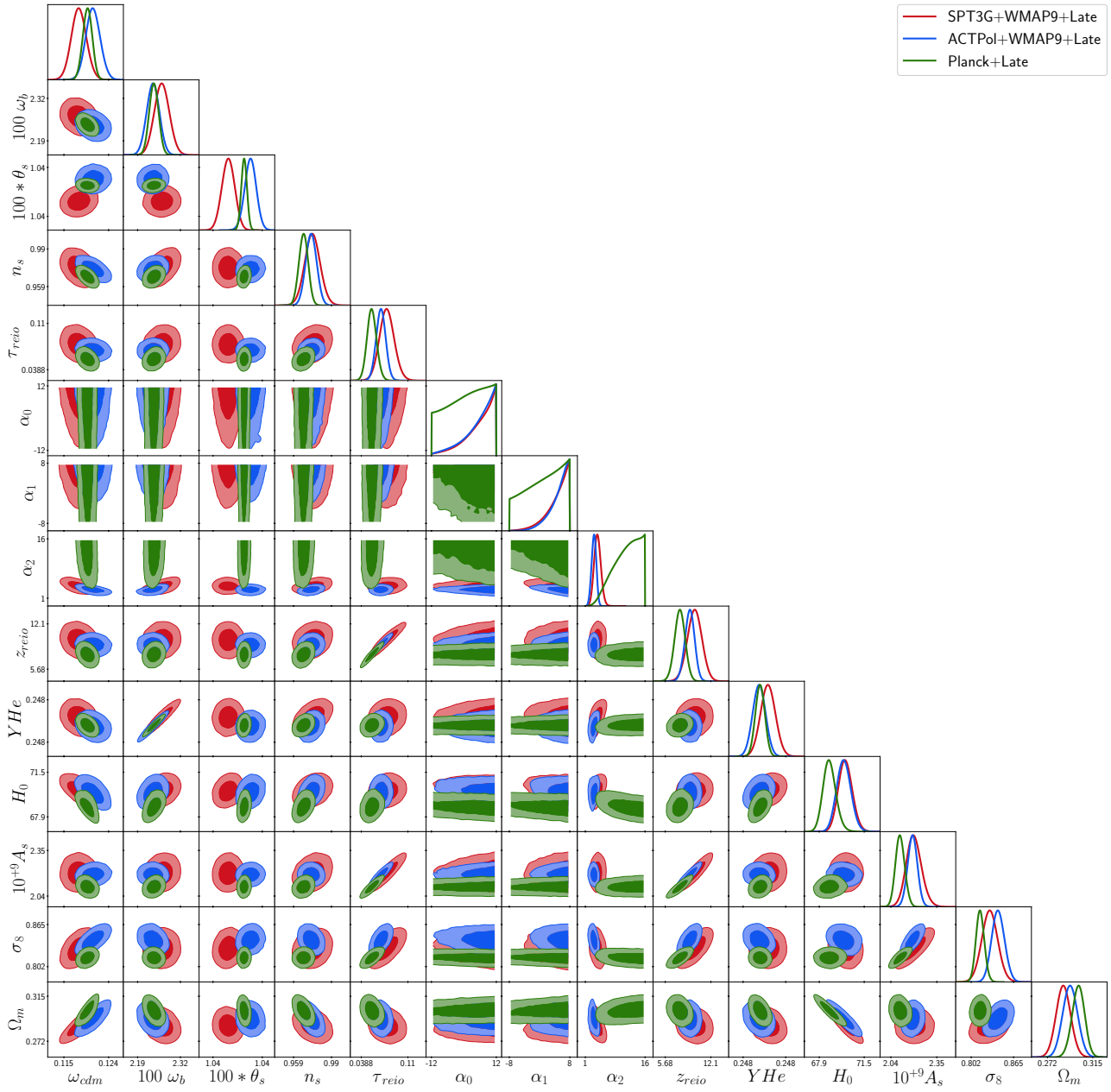

Figure 1. 1σ and 2σ confidence contours for the phantom scalar field cosmological parameters. We present the results for our three baselines: Planck 2018+BAO+Pantheon+Cosmic clocks, SPT-3G+WMAP9+BAO+Pantheon+Cosmic clocks, and ACTPol DR-4+WMAP9+BAO+Pantheon+Cosmic clocks.

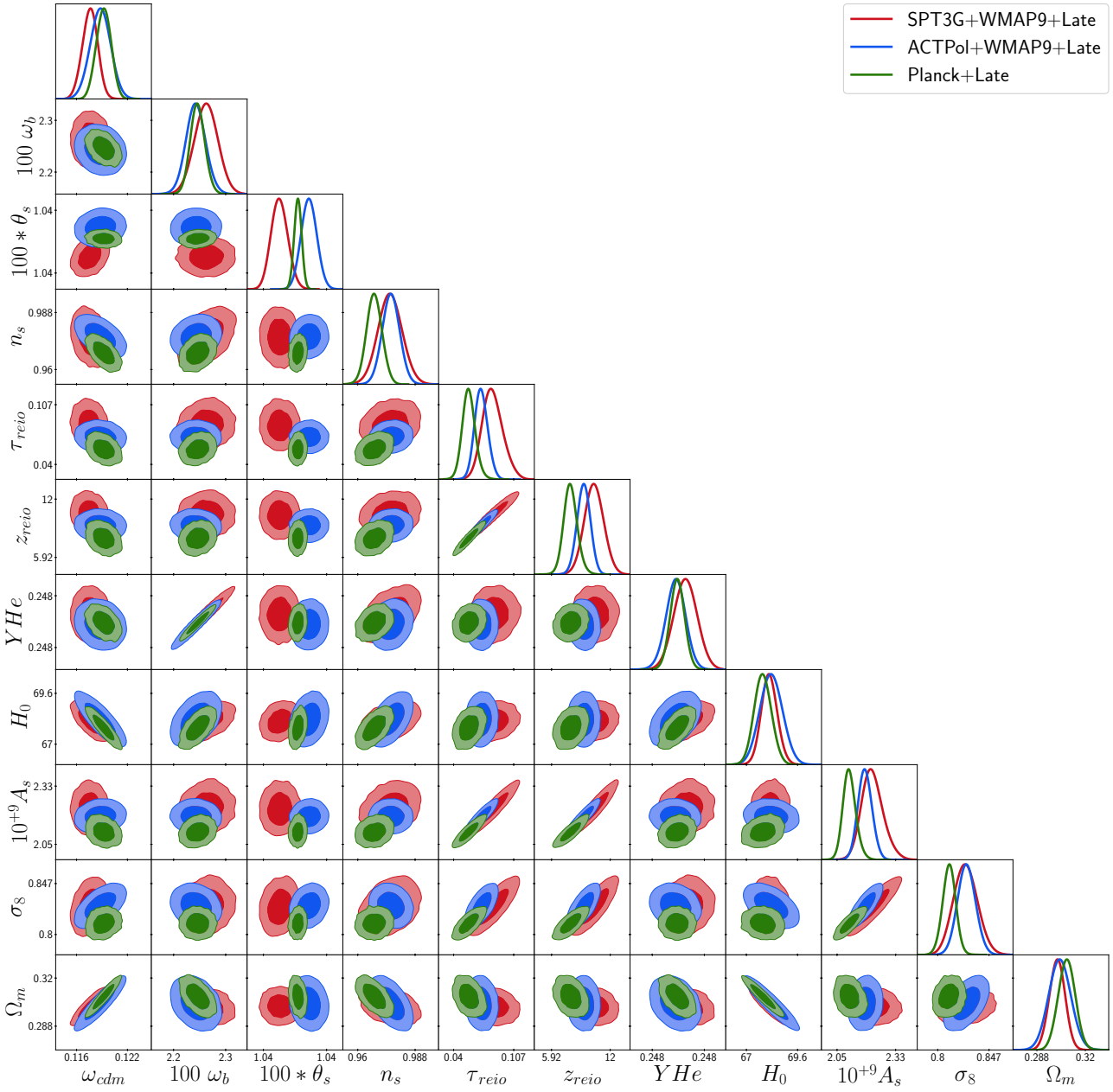

Figure 2. 1σ and 2σ confidence contours for the ΛCDM cosmological parameters. We present the results for the same baselines as for the phantom scalar field.

To visualize these results, we present Figure 3. We included the results of the Hubble constant for the phantom scalar field (abbreviated as SF) and ΛCDM for the three baselines considered. We also included the result from [51] of this model by using a compressed Planck likelihood. Finally, we included the mean values and uncertainties at 1σ for Planck 2018 [15] and SH0ES 2022 [52]. As we can see, ΛCDM is consistent with Planck 2018 for the three baselines and it is in tension with SH0ES 2022. On the other hand, the phantom scalar field gets a higher value of H_0 that departs from the ΛCDM value but does not get high enough to be fully consistent with SH0ES 2022. However, other phantom scalar field models might be consistent with a higher H_0 by choosing a different parametrization of y_2 or a different potential.

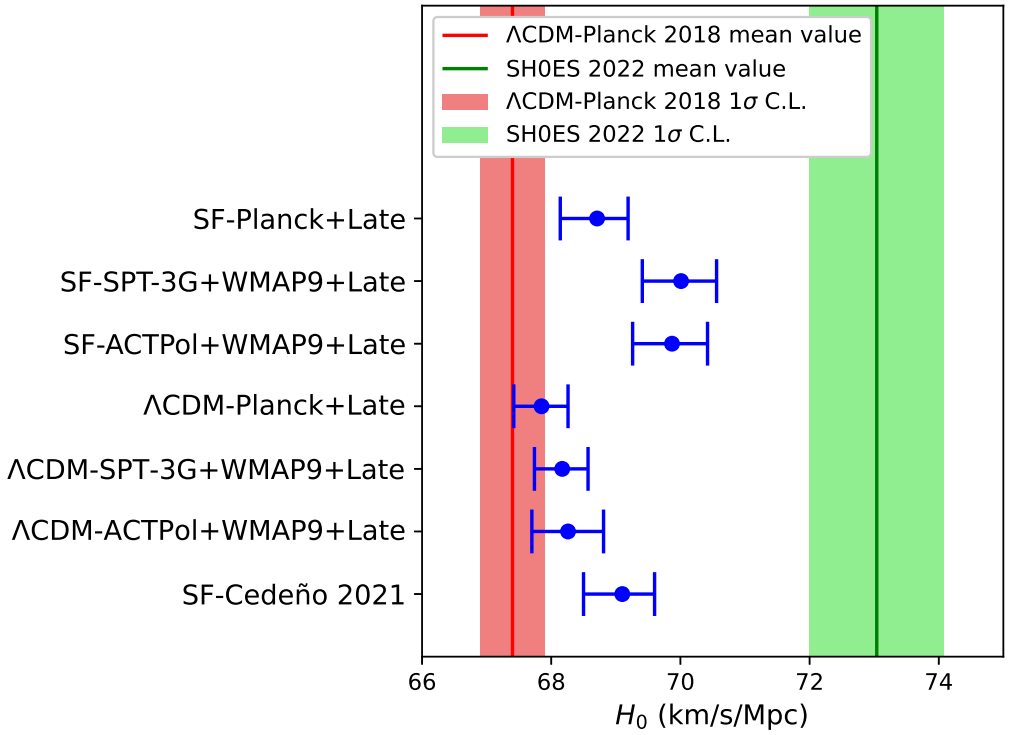

Figure 3. Whisker plot with the mean values and uncertainties at 1σ C.L. for the phantom scalar field (abbreviated as SF) and the ΛCDM models and the three baselines described. We also included the mean value and uncertainty at 1σ C.L. from the latest results from SH0ES collaboration [52] and Planck 2018 [15] to study the Hubble tension. A result from [51] was added for comparison.

5. Conclusions

In this work, we studied new early constraints on tracker phantom scalar field cosmologies, in particular, some solutions regarding the proposal discussed in [51]. We focused on the case where the late-time accelerated expansion of the universe is solely caused by a scalar field without the assistance of a cosmological constant. We employed early-time catalogs regarding CMB measurements and a full late-time catalog, which includes SNIa, Cosmick clocks, and BAO observables. For these models, the EoS of the scalar field gives $w < -1$, which enables a larger cosmic late-time expansion and, then, a possibly higher value of H_0.

We considered four CMB catalogs: Planck 2018, WMAP9, SPT-3G, and ACTPol DR-4, alongside late-time catalogs. Our methodology in this part consisted of constraining the tracker phantom scalar field using three different baselines: Planck+Late, STP-3G+WMAP9+Late, and ACTPol+WMAP9+Late (where *late* stands for the late-time catalogs). To compare our results, we computed the constraints with ΛCDM as a baseline model. The free parameters of the scalar field, named α_0, α_1, and α_2 from Equation (13), did not fully converge for the Planck 2018 baseline. For the remaining baselines, α_0, and α_1 did not obtain a full convergence. However, they showed a good performance for the case of α_2. The remaining cosmological parameters of the model showed good convergence for all the baselines and both the scalar field and ΛCDM models.

We were particularly interested in the constraints on the Hubble constant H_0 to study its statistical tension. For the Planck 2018 catalog, the scalar field model shows a tension higher than 4σ C.L. when compared with the latest result from the SH0ES collaboration [52]. This result shows that these phantom scalar field models do not fully address the tension when considering the latest Planck 2018 results, which differs from the one reported in [51]. However, for the model-independent baselines employed in this work (SPT-3G+WMAP9+Late and ACTPol+WMAP9+Late), the H_0 tension was reduced to below 3σ C.L, without altering the σ_8 value. This result shows that phantom scalar field models

can reduce the H_0 constant tension when considering CMB model-independent baselines. However, it is important to mention that this particular model cannot completely solve the tension issue since the tension is not lower than 2σ. Our results are interesting since CMB baselines with model-dependent/independent characteristics can lead to different conclusions regarding cosmological tensions. Planck 2018 data points out that the tracker model does not address the tension, while SPT-3G, ACTPol DR-4, and WMAP9 baselines hint that phantom scalar field models reduce the tension, but without solving it completely. Thus, the analyses carried out in this work are inconclusive on whether phantom scalar field models can solve the Hubble constant problem. Furthermore, new definitions in (7) might lower the statistical tension at early times, e.g., from the ones reported in [37]. These models might achieve a lower tension with SH0ES 2022 [52] and they would also need to predict a higher value of H_0 with the Planck 2018 baseline. This is possible due to the EoS of phantom fields ($w < -1$) that can drive a faster late-time expansion of the universe. This aspect will be reported elsewhere.

Author Contributions: Conceptualization, C.E.-R.; Formal analysis, J.A.N. and C.E.-R.; Investigation, J.A.N. and C.E.-R.; Methodology, J.A.N. and C.E.-R.; Resources, C.E.-R.; Software, J.A.N.; Supervision, C.E.-R.; Validation, J.A.N. and C.E.-R.; Visualization, J.A.N.; Writing—original draft, J.A.N. and C.E.-R.; Writing—review & editing, J.A.N. and C.E.-R. All authors have read and agreed to the published version of the manuscript

Funding: C.E.-R. was supported by the CONACyT Network Project No. 376127 and the authors acknowledge the Royal Astronomical Society as Fellow FRAS 10147. This research was carried out using computational facilities procured through the Cosmostatistics National Group ICN UNAM project. This article is based upon work from COST Action CA21136 Addressing observational tensions in cosmology with systematics and fundamental physics (CosmoVerse) supported by COST (European Cooperation in Science and Technology). J.A.N. acknowledges financial support from the "Excellence Project Scholarship" funded by the Physics and Astronomy Department of the University of Padova.

Data Availability Statement: No new data were created in this study. Date sharing is not applicable to this article.

Conflicts of Interest: The Authors declare no conflicts of interest.

Abbreviations

The following abbreviations are used in this manuscript:

ΛCDM	Lambda cold dark matter
CMB	Cosmic Microwave Background
SNeIa	Type Ia Supernovae
BAOs	Baryon Acoustic Oscillations

References

1. Perlmutter, S.; Aldering, G.; Goldhaber, G.; Knop, R.A.; Nugent, P.; Castro, P.G.; Deustua, S.; Fabbro, S.; Goobar, A.; Groom, D.E.; et al. Measurements of Ω and Λ from 42 high redshift supernovae. *Astrophys. J.* **1999**, *517*, 565–586. [CrossRef]
2. Riess, A.G.; Filippenko, A.V.; Challis, P.; Clocchiatti, A.; Diercks, A.; Garnavich, P.M.; Gilliland, R.L.; Hogan, C.J.; Jha, S.; Kirshner, R.P.; et al. Observational evidence from supernovae for an accelerating universe and a cosmological constant. *Astron. J.* **1998**, *116*, 1009–1038. [CrossRef]
3. Jaffe, A.H.; Ade, P.A.R.; Balbi, A.; Bock, J.J.; Bond, J.R.; Borrill, J.; Boscaleri, A.; Coble, K.; Crill, B.P.; de Bernardis, P.; et al. Cosmology from MAXIMA-1, BOOMERANG and COBE/DMR CMB observations. *Phys. Rev. Lett.* **2001**, *86*, 3475–3479. [CrossRef]
4. Eisenstein, D.J.; Zehavi, I.; Hogg, D.W.; Scoccimarro, R.; Blanton, M.R.; Nichol, R.C.; Scranton, R.; Seo, H.-J.; Tegmark, M.; Zheng, Z.; et al. Detection of the Baryon Acoustic Peak in the Large-Scale Correlation Function of SDSS Luminous Red Galaxies. *Astrophys. J.* **2005**, *633*, 560–574. [CrossRef]
5. Anderson, L.; Aubourg, E.; Bailey, S.; Beutler, F.; Bhardwaj, V.; Blanton, M.; Bolton, A.S.; Brinkmann, J.; Brownstein, J.R.; Burden, A.; et al. The clustering of galaxies in the SDSS-III Baryon Oscillation Spectroscopic Survey: Baryon acoustic oscillations in the Data Releases 10 and 11 Galaxy samples. *Mon. Not. Roy. Astron. Soc.* **2014**, *441*, 24–62. [CrossRef]

6. Abbott, T.M.C.; Abdalla, F.B.; Alarcon, A.; Allam, S.; Allen, S.; Amara, A.; Annis, J.; Asorey, J.; Avila, S.; Bacon, D.; et al. Dark Energy Survey year 1 results: Cosmological constraints from galaxy clustering and weak lensing. *Phys. Rev. D* **2018**, *98*, 043526. [CrossRef]
7. Brout, D.; Scolnic, D.; Popovic, B.; Riess, A.G.; Carr, A.; Zuntz, J.; Kessler, R.; Davis, T.M.; Hinton, S.; Jones, D.; et al. The Pantheon+ Analysis: Cosmological Constraints. *Astrophys. J.* **2022**, *938*, 110. [CrossRef]
8. Scolnic, D.; Perlmutter, S.; Aldering, G.; Brout, D.; Davis, T.; Filippenko, A.; Foley, R.; Hlozek, R.; Hounsell, R.; Jha, S.; et al. The Next Generation of Cosmological Measurements with Type Ia Supernovae. *arXiv* **2019**, arXiv:1903.05128. https://doi.org/10.48550/arXiv.1903.05128.
9. Lu, J.; Wang, L.; Chen, X.; Rubin, D.; Perlmutter, S.; Baade, D.; Mould, J.; Vinko, J.; Regős, E.; Koekemoer, A.M. Constraints on Cosmological Parameters with a Sample of Type Ia Supernovae from JWST. *Astrophys. J.* **2022**, *941*, 71. [CrossRef]
10. Di Valentino, E.; Anchordoqui, L.A.; Akarsu, O.; Ali-Haimoud, Y.; Amendola, L.; Arendse, N.; Asgari, M.; Ballardini, M.; Basilakos, S.; Battistelli, E.; et al. Cosmology Intertwined III: $f\sigma_8$ and S_8. *Astropart. Phys.* **2021**, *131*, 102604. [CrossRef]
11. Di Valentino, E.; Melchiorri, A.; Silk, J. Planck evidence for a closed Universe and a possible crisis for cosmology. *Nat. Astron.* **2019**, *4*, 196–203. [CrossRef]
12. Handley, W. Curvature tension: Evidence for a closed universe. *Phys. Rev. D* **2021**, *103*, L041301. [CrossRef]
13. Di Valentino, E.; Anchordoqui, L.A.; Akarsu, O.; Ali-Haimoud, Y.; Amendola, L.; Arendse, N.; Asgari, M.; Ballardini, M.; Basilakos, S.; Battistelli, E.; et al. Snowmass2021—Letter of interest cosmology intertwined IV: The age of the universe and its curvature. *Astropart. Phys.* **2021**, *131*, 102607. [CrossRef]
14. Di Valentino, E.; Anchordoqui, L.A.; Akarsu, Ö.; Ali-Haimoud, Y.; Amendola, L.; Arendse, N.; Asgari, M.; Ballardini, M.; Basilakos, S.; Battistelli, E.; et al. Snowmass2021—Letter of interest cosmology intertwined II: The hubble constant tension. *Astropart. Phys.* **2021**, *131*, 102605. [CrossRef]
15. Aghanim, N.; Anchordoqui, L.A.; Akarsu, O.; Ali-Haimoud, Y.; Amendola, L.; Arendse, N.; Asgari, M.; Ballardini, M.; Basilakos, S.; Battistelli, E.; et al. Planck 2018 results. VI. Cosmological parameters. *Astron. Astrophys.* **2020**, *641*, A6, Erratum in *Astron. Astrophys.* **2021**, *652*, C4. [CrossRef]
16. Abdalla, E.; Abellán, G.F.; Aboubrahim, A.; Agnello, A.; Akarsu, O.; Akrami, Y.; Alestas, G.; Aloni, D.; Amendola, L.; Anchordoqui, L.A.; et al. Cosmology intertwined: A review of the particle physics, astrophysics, and cosmology associated with the cosmological tensions and anomalies. *JHEAp* **2022**, *34*, 49–211. [CrossRef]
17. Abbott, T.; Abdalla, F.B.; Aleksic, J.; Allam, A.; Amara, A.; Bacon, D.; Balbinot, E.; Banerji, M.; Bachtol, K.; Bernstein, M.; et al. The Dark Energy Survey: More than dark energy—An overview. *Mon. Not. Roy. Astron. Soc.* **2016**, *460*, 1270–1299. [CrossRef]
18. Aghamousa, A.; Aguilar, J.; Ahlen, S.; Alam, S.; Allen, L.E.; Prieto, C.A.; Annis, J.; Bailey, S.; Balland, C.; Ballester, O.; et al. The DESI Experiment Part I: Science,Targeting, and Survey Design. *arXiv* **2016**, arXiv:1611.00036.
19. Mandelbaum, R.; Eifler, T.; Hlozek, R.; Collett, T.; Gawiser, E.; Scolnic, D.; Alonso, D.; Awan, H.; Biswas, R.; Blazek, J.; et al. The LSST Dark Energy Science Collaboration (DESC) Science Requirements Document. *arXiv* **2018**, arXiv:1809.01669.
20. Amendola, L.; Appleby, S.; Avgoustidis, A.; Bacon, D.; Baker, T.; Baldi, M.; Bartolo, N.; Blanchard, A.; Bonvin, C.; Borgani, S.; et al. Cosmology and fundamental physics with the Euclid satellite. *Living Rev. Relativ.* **2018**, *21*, 2. [CrossRef]
21. Aiola, S.; Calabrese, E.; Maurin, L.; Naess, S.; Schmitt, B.L.; Abitbol, M.H.; Addison, G.E.; Ade, P.A.; Alonso, D.; Amiri, M.; et al. The Atacama Cosmology Telescope: DR4 maps and cosmological parameters. *J. Cosmol. Astropart. Phys.* **2020**, *2020*, 047. [CrossRef]
22. Dutcher, D.; Balkenhol, L.; Ade, P.; Ahmed, Z.; Anderes, E.; Anderson, A.; Archipley, M.; Avva, J.; Aylor, K.; Barry, P.; et al. Measurements of the E-mode polarization and temperature-E-mode correlation of the CMB from SPT-3G 2018 data. *Phys. Rev. D* **2021**, *104*, 022003. [CrossRef]
23. Escamilla-Rivera, C.; Capozziello, S. Unveiling cosmography from the dark energy equation of state. *Int. J. Mod. Phys. D* **2019**, *28*, 1950154. [CrossRef]
24. Escamilla-Rivera, C. Status on bidimensional dark energy parameterizations using SNe Ia JLA and BAO datasets. *Galaxies* **2016**, *4*, 8. [CrossRef]
25. Escamilla, L.A.; Giarè, W.; Di Valentino, E.; Nunes, R.C.; Vagnozzi, S. The state of the dark energy equation of state circa 2023. *arXiv* **2023**, arXiv:2307.14802.
26. Escamilla-Rivera, C.; Nájera, A. Dynamical dark energy models in the light of gravitational-wave transient catalogues. *JCAP* **2022**, *3*, 060. [CrossRef]
27. Escamilla-Rivera, C.; Quintero, M.A.C.; Capozziello, S. A deep learning approach to cosmological dark energy models. *JCAP* **2020**, *3*, 008. [CrossRef]
28. Zhang, H.C. Dynamical dark energy can amplify the expansion rate of the Universe. *Phys. Rev. D* **2023**, *107*, 103529. [CrossRef]
29. Jaime, L.G.; Jaber, M.; Escamilla-Rivera, C. New parametrized equation of state for dark energy surveys. *Phys. Rev. D* **2018**, *98*, 083530. [CrossRef]
30. Clifton, T.; Ferreira, P.G.; Padilla, A.; Skordis, C. Modified Gravity and Cosmology. *Phys. Rep.* **2012**, *513*, 1–189. [CrossRef]
31. Amendola, L.; Gannouji, R.; Polarski, D.; Tsujikawa, S. Conditions for the cosmological viability of f(R) dark energy models. *Phys. Rev. D* **2007**, *75*, 083504. [CrossRef]
32. Bahamonde, S.; Dialektopoulos, K.F.; Escamilla-Rivera, C.; Farrugia, G.; Gakis, V.; Hendry, M.; Hohmann, M.; Levi Said, J.; Mifsud, J.; Di Valentino, E. Teleparallel gravity: From theory to cosmology. *Rept. Prog. Phys.* **2023**, *86*, 026901. [CrossRef]

33. de Ritis, R.; Marino, A.A.; Rubano, C.; Scudellaro, P. Quintessence duality. *Int. J. Mod. Phys. D* **2001**, *10*, 921–926. [CrossRef]
34. Alho, A.; Uggla, C.; Wainwright, J. Tracking Quintessence. *Phys. Dark Univ.* **2024**, *44*, 101433. [CrossRef]
35. Banerjee, A.; Cai, H.; Heisenberg, L.; Colgáin, E.Ó.; Sheikh-Jabbari, M.M.; Yang, T. Hubble sinks in the low-redshift swampland. *Phys. Rev. D* **2021**, *103*, L081305. [CrossRef]
36. Lee, B.H.; Lee, W.; Colgáin, E.Ó.; Sheikh-Jabbari, M.; Thakur, S. Is local H 0 at odds with dark energy EFT? *J. Cosmol. Astropart. Phys.* **2022**, *2022*, 004. [CrossRef]
37. Cai, Y.F.; Saridakis, E.N.; Setare, M.R.; Xia, J.Q. Quintom cosmology: Theoretical implications and observations. *Phys. Rep.* **2010**, *493*, 1–60. [CrossRef]
38. Setare, M.; Saridakis, E. Coupled oscillators as models of quintom dark energy. *Phys. Lett. B* **2008**, *668*, 177–181. [CrossRef]
39. Bamba, K.; Capozziello, S.; Nojiri, S.; Odintsov, S.D. Dark energy cosmology: The equivalent description via different theoretical models and cosmography tests. *Astrophys. Space Sci.* **2012**, *342*, 155–228. [CrossRef]
40. Teng, Y.P.; Lee, W.; Ng, K.W. Constraining the dark-energy equation of state with cosmological data. *Phys. Rev. D* **2021**, *104*, 083519. [CrossRef]
41. Gangopadhyay, M.R.; Sami, M.; Sharma, M.K. Phantom dark energy as a natural selection of evolutionary processes â la genetic algorithm and cosmological tensions. *Phys. Rev. D* **2023**, *108*, 103526. [CrossRef]
42. Yashar, M.; Bozek, B.; Abrahamse, A.; Albrecht, A.; Barnard, M. Exploring Parameter Constraints on Quintessential Dark Energy: The Inverse Power Law Model. *Phys. Rev. D* **2009**, *79*, 103004. [CrossRef]
43. Ureña López, L.A.; Roy, N. Generalized tracker quintessence models for dark energy . *Phys. Rev. D* **2020**, *102*, 063510. [CrossRef]
44. Roy, N.; Ureña López, L.A. Tracker behaviour of quintom dark energy and the Hubble tension. *arXiv* **2023**, arXiv:2312.04003.
45. Adil, A.; Albrecht, A.; Knox, L. Quintessential cosmological tensions. *Phys. Rev. D* **2023**, *107*, 063521. [CrossRef]
46. Copeland, E.J.; Moss, A.; Sevillano Muñoz, S.; White, J.M.M. Scaling solutions as Early Dark Energy resolutions to the Hubble tension. *arXiv* **2023**, arXiv:2309.15295.
47. Caldwell, R.R. A phantom menace? Cosmological consequences of a dark energy component with super-negative equation of state. *Phys. Lett. B* **2002**, *545*, 23–29. [CrossRef]
48. Ratra, B.; Peebles, P.J. Cosmological consequences of a rolling homogeneous scalar field. *Phys. Rev. D* **1988**, *37*, 3406. [CrossRef]
49. Steinhardt, P.J.; Wang, L.; Zlatev, I. Cosmological tracking solutions. *Phys. Rev. D* **1999**, *59*, 123504. [CrossRef]
50. Roy, N.; Gonzalez-Morales, A.X.; Ureña-López, L.A. New general parametrization of quintessence fields and its observational constraints. *Phys. Rev. D* **2018**, *98*, 063530. [CrossRef]
51. Cedeño, F.X.L.; Roy, N.; Ureña-López, L.A. Tracker phantom field and a cosmological constant: Dynamics of a composite dark energy model. *Phys. Rev. D* **2021**, *104*, 123502. [CrossRef]
52. Riess, A.G.; Yuan, W.; Macri, L.M.; Scolnic, D.; Brout, D.; Casertano, S.; Jones, D.O.; Murakami, Y.; Anand, G.S.; Breuval, L.; et al. A Comprehensive Measurement of the Local Value of the Hubble Constant with 1 km s- 1 Mpc- 1 Uncertainty from the Hubble Space Telescope and the SH0ES Team. *Astrophys. J. Lett.* **2022**, *934*, L7. [CrossRef]
53. Hinshaw, G.; Larson, D.; Komatsu, E.; Spergel, D.N.; Bennett, C.; Dunkley, J.; Nolta, M.; Halpern, M.; Hill, R.; Odegard, N.; et al. Nine-year Wilkinson Microwave Anisotropy Probe (WMAP) observations: Cosmological parameter results. *Astrophys. J. Suppl. Ser.* **2013**, *208*, 19. [CrossRef]
54. Blas, D.; Lesgourgues, J.; Tram, T. The cosmic linear anisotropy solving system (CLASS). Part II: Approximation schemes. *J. Cosmol. Astropart. Phys.* **2011**, *2011*, 034. [CrossRef]
55. Audren, B.; Lesgourgues, J.; Benabed, K.; Prunet, S. Conservative constraints on early cosmology with MONTE PYTHON. *J. Cosmol. Astropart. Phys.* **2013**, *2013*, 001. [CrossRef]
56. Brinckmann, T.; Lesgourgues, J. MontePython 3: Boosted MCMC sampler and other features. *Phys. Dark Universe* **2019**, *24*, 100260. [CrossRef]
57. Scolnic, D.M.; Jones, D.; Rest, A.; Pan, Y.; Chornock, R.; Foley, R.; Huber, M.; Kessler, R.; Narayan, G.; Riess, A.; et al. The complete light-curve sample of spectroscopically confirmed SNe Ia from Pan-STARRS1 and cosmological constraints from the combined pantheon sample. *Astrophys. J.* **2018**, *859*, 101. [CrossRef]
58. Jimenez, R.; Loeb, A. Constraining cosmological parameters based on relative galaxy ages. *Astrophys. J.* **2002**, *573*, 37. [CrossRef]
59. Moresco, M.; Pozzetti, L.; Cimatti, A.; Jimenez, R.; Maraston, C.; Verde, L.; Thomas, D.; Citro, A.; Tojeiro, R.; Wilkinson, D. A 6% measurement of the Hubble parameter at z 0.45: Direct evidence of the epoch of cosmic re-acceleration. *J. Cosmol. Astropart. Phys.* **2016**, *2016*, 014. [CrossRef]
60. Alam, S.; Ata, M.; Bailey, S.; Beutler, F.; Bizyaev, D.; Blazek, J.A.; Bolton, A.S.; Brownstein, J.R.; Burden, A.; Chuang, C.H.; et al. The clustering of galaxies in the completed SDSS-III Baryon Oscillation Spectroscopic Survey: Cosmological analysis of the DR12 galaxy sample. *Mon. Not. R. Astron. Soc.* **2017**, *470*, 2617–2652. [CrossRef]
61. Chudaykin, A.; Gorbunov, D.; Nedelko, N. Exploring Λ CDM extensions with SPT-3G and Planck data: 4σ evidence for neutrino masses, full resolution of the Hubble crisis by dark energy with phantom crossing, and all that. *arXiv* **2022**, arXiv:2203.03666.

62. Gelman, A.; Rubin, D.B. Inference from iterative simulation using multiple sequences. *Stat. Sci.* **1992**, *7*, 457–472. [CrossRef]
63. Sharma, M.K.; Pacif, S.K.J.; Yergaliyeva, G.; Yesmakhanova, K. The Oscillatory Universe, phantom crossing and the Hubble tension. *Ann. Phys.* **2023**, *454*, 169345. [CrossRef]